

Surface tension effects for particle settling and resuspension in viscous thin films

A. Mavromoustaki,¹ L. Wang,² J. Wong*,^{3,1} and A. L. Bertozzi¹

¹*Department of Mathematics, University of California Los Angeles,
520 Portola Plaza, Los Angeles, CA 90095, USA*

²*Department of Mathematics, State University of Buffalo at New York, Buffalo, NY 14260*

³*Department of Mathematics, Duke University,
120 Science Drive, Durham, NC 27708, USA*

(Dated: March 13, 2018)

We consider flow of a thin film on an incline with negatively buoyant particles. We derive a one-dimensional lubrication model, including the effect of surface tension, which is a nontrivial extension of a previous model (Murisic *et. al* [J. Fluid Mech. 2013]). We show that the surface tension, in the form of high order derivatives, not only regularizes the previous model as a high order diffusion, but also modifies the fluxes. As a result, it leads to a different stratification in the particle concentration along the direction perpendicular to the motion of the fluid mixture. The resulting equations are of mixed hyperbolic-parabolic type and different from the well-known lubrication theory for a clear fluid or fluid with surfactant. To study the system numerically, we formulate a semi-implicit scheme that is able to preserve the particle maximum packing fraction. We show extensive numerical results for this model including a qualitative comparison with two-dimensional laboratory experiments.

I. INTRODUCTION

Recent development in thin-film flows involves studying the dynamics of films laden with particles flowing down an inclined plane [7, 8, 20, 29, 32]. Understanding the underlying physics of these flows is important to a number of industrial and geophysical applications such as food processing [19], coating flow technologies [6], and landslides and debris flow [14]. These require efficient handling of solids in slurries and uniform particle distributions. The first thin-film model of particle-laden flow with a free surface is attributed to Zhou *et al.* [32], wherein both the effects of hindered settling and surface tension are included and rescaled properly to account for their physical significance. This model captures the ‘ridged’ regime in which particles accumulate at a single, particle-rich front. However, the model assumes a rapid vertical diffusion in the bulk of the fluid, and thereby fails to capture a dominant flow pattern observed in experiments up to moderate particle concentrations: the ‘settled’ regime in which particles settle towards the substrate and a clear fluid layer flows over them. In subsequent studies [7, 9], the mathematical model was improved through the addition of shear-induced migration, which suggested a balance between hindered settling and shear-induced migration as the dominant large scale physics for particle/liquid separation. The improved equilibrium model was used by Murisic *et. al.* [20] to successfully predict the critical concentration where the suspension transitions from the ‘settled’ to the ‘ridged’ regime, which depends on the inclination angle and relative density of particles to fluid. At the critical concentration is an unstable equilibrium (the ‘mixed’ regime) for which the particles remain uniformly mixed.

The most recent dynamic model based on lubrication theory was proposed by Murisic *et. al.* in [21]. The derivation follows an asymptotic analysis of the underlying governing equations in the lubrication limit, incorporating the effects of hindered settling and shear-induced migration but omitting surface tension. The resulting equations form a hyperbolic system of conservation laws for the film height and integrated particle concentration. This system is extensively analyzed in the following studies [17, 27, 28]; typical solutions are shown to be a pair of shocks (for separated fluid and particle wave fronts) in the settled regime and either a double shock or a singular shock in the ridged regime. The singular shock, in which the particle concentration achieves the maximum packing fraction, is a novel feature which suggests the accumulation of particles at the particle-rich ridge.

While previous models have been successful in capturing the dynamics of the bulk flow, they do not provide a description of the detailed structure of the fluid front. Near the front, surface tension becomes

* Corresponding author. Email: jtwong@math.duke.edu

a dominant effect, leading to the growth of a capillary ridge and fingering instabilities [13]. In this paper, we introduce a model for particle-laden flow with surface tension, extending the model of Murisic *et al.* As we will demonstrate, there are subtle issues in constructing the model, so we focus on the one dimensional case where the spanwise variation is neglected. Even in one dimension, the addition of surface tension and the presence of particles will significantly change the type of the model due to the complicated *nonlinear* dependence of the fluid and particle fluxes on the pressure gradient. In the next section, we describe in detail the derivation of the mathematical model by taking into account the surface tension effect. In Section III, we derive the equations in the dilute limit (i.e. where the particle concentration is very small), for which the equations have an explicit form. In Section IV, we propose a semi-implicit numerical scheme for the new model, taking special care to consistently discretizing both the fluid and particle equations so that the particle concentration does not exceed the maximum packing fraction. Some numerical simulations are carried out in Section V, where we compare the solutions with and without surface tension and provide a preliminary comparison with experimental data. Finally, the paper is concluded in Section VI, where we discuss some open questions and directions for future research.

II. MATHEMATICAL MODEL

A. Evolution equations

In this section, we derive a lubrication model including the effect of surface tension. The derivation follows that in [21] with significant changes to account for the dependence of the particle distribution and fluid velocity on the surface tension. Consider a flow in a rectangular, rigid channel inclined at an angle α to the horizontal in a two-dimensional coordinate system (x, z) , where x and z represent the axial and normal directions to the flow, respectively (see Fig. 1). Here we ignore the span-wise direction to more clearly

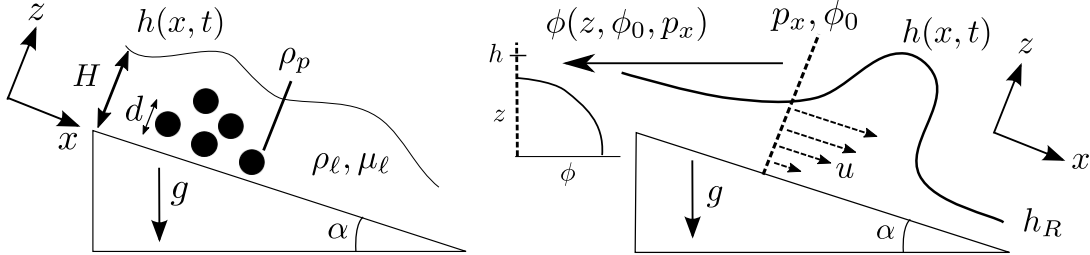


Figure 1: Sketches of the setup. Left: physical parameters and scalings. Right: ‘equilibrium’ scheme; at each point x along the incline there is an equilibrium particle distribution $\phi(z, \phi_0, p_x)$ in the z -direction depending on the depth-averaged concentration $\phi_0(x, t)$ and pressure gradient $p_x(x, t)$.

illustrate the the surface tension effect. The mixture is comprised of a fluid with density ρ_ℓ and particles with density $\rho_p > \rho_\ell$. We model the mixture as a single (quasi)-Newtonian fluid with a concentration-dependent density $\rho(\phi)$ and viscosity $\mu(\phi)$. The dynamics of this flow are governed by the incompressible Navier-Stokes equations

$$\begin{cases} \rho(\phi)(\mathbf{u}_t + \mathbf{u} \cdot \nabla \mathbf{u}) = -\nabla p + \nabla \cdot (\mu(\phi) (\nabla \mathbf{u}^T + \nabla \mathbf{u})) + \rho(\phi) \mathbf{g}, \\ \nabla \cdot \mathbf{u} = 0. \end{cases} \quad (1a) \quad (1b)$$

Here $\mathbf{u} = (u, w)$ represents the velocity field and $\mathbf{g} = (g \sin \alpha, -g \cos \alpha)$. The mixture density is $\rho(\phi) = (1 - \phi)\rho_\ell + \phi\rho_p$ and we use the Krieger-Dougherty relation $\mu(\phi) = (1 - \phi/\phi_m)^{-2}$ with ϕ_m the maximum packing fraction (taken to be $\phi_m = 0.61$). The particle concentration $\phi(x, z, t)$ satisfies a transport equation which takes into account migration due to advection and flux gradients. It reads

$$\partial_t \phi + \mathbf{u} \cdot \nabla \phi + \nabla \cdot \mathbf{J} = 0, \quad (2)$$

where the flux $\mathbf{J} = (J_1, J_3)$ represents the total flux of particles due to gravity and shear-induced migration arising from particle collisions. Solutions of the equations are subject to the no-slip boundary condition and

continuity of the velocity and stress:

$$\begin{cases} u(z=0) = 0, & \mu u_z(z=h) = 0, \\ p(z=h) = P_0 - \gamma_0 \kappa, \end{cases} \quad \begin{matrix} (3a) \\ (3b) \end{matrix}$$

where P_0 is the atmospheric pressure, κ is the curvature of the surface and γ_0 is the surface tension, which is considered constant in this work. To justify this assumption, a series of experiments were carried out in the physical regime of interest, detailed in Appendix A. The flux satisfies the no-flux boundary condition $\mathbf{J} \cdot \mathbf{n} = 0$ at $z = 0$ and $z = h$, which implies that the model does not allow for particles to adsorb at the interface.

Proceeding with the formulation of our model, we introduce the following scalings to render the governing equations dimensionless:

$$\begin{aligned} \hat{x} &= \frac{x}{L}, & \hat{z} &= \frac{z}{H}, & \hat{h} &= \frac{h}{H}, & H &= \epsilon L, & \hat{u} &= \frac{u}{U}, & \hat{w} &= \frac{w}{\epsilon U}, & \hat{t} &= \frac{tU}{L}, \\ \hat{p} &= \frac{p}{P}, & \hat{\mu} &= \frac{\mu}{\mu_l}, & \hat{\rho} &= \frac{\rho}{\rho_l} = 1 + \frac{\rho_p - \rho_l}{\rho_l} \phi = 1 + \rho_s \phi, \end{aligned}$$

where the quantities shown with a hat are dimensionless and $\epsilon \ll 1$ represents the lubrication parameter. The driving mechanism for the flow is gravitational and therefore, it follows from a balance between gravity and viscosity terms that $\rho_l g \sin \alpha = \mu_l U / (\epsilon^2 L^2)$, which leads to the velocity scale $U = \rho_l g \sin \alpha H^2 / \mu_l$. For highly viscous flows, it is appropriate to scale the pressure according to $P/L = \mu_l U / H^2$.

We note that in this setting, the viscous terms are dominant compared to the inertial terms and hence the Reynolds number, $\text{Re} = \rho_l U L / \mu_l \ll 1$ which implies that inertial contributions in (1a) can be ignored. Rewriting (1a) in terms of the dimensionless variables, we have

$$\rho_l U \hat{\rho} \left(\frac{\hat{u}_{\hat{t}}}{\hat{T}} + \frac{U}{L} \hat{u} \hat{u}_{\hat{x}} + \frac{\epsilon U}{H} \hat{w} \hat{u}_{\hat{z}} \right) = -\frac{P}{L} \hat{p}_{\hat{x}} + \frac{2\mu_l U}{L^2} (\hat{\mu} \hat{u}_{\hat{x}})_{\hat{x}} + \frac{\mu_l U}{H^2} (\hat{\mu} (\hat{u}_{\hat{z}} + \hat{w}_{\hat{x}}))_{\hat{z}} + \rho_l \hat{\rho} g \sin \alpha, \quad (4)$$

and

$$\rho_l U \hat{\rho} \left(\frac{\epsilon \hat{w}_{\hat{t}}}{\hat{T}} + \frac{\epsilon U}{L} \hat{u} \hat{w}_{\hat{x}} + \frac{\epsilon^2 U^2}{H} \hat{w} \hat{w}_{\hat{z}} \right) = -\frac{P}{H} \hat{p}_{\hat{z}} + \frac{2\epsilon \mu_l U}{H^2} (\hat{\mu} \hat{w}_{\hat{z}})_{\hat{z}} + \frac{\mu_l U}{L^2} (\hat{\mu} (\frac{1}{\epsilon} \hat{u}_{\hat{z}} + \epsilon \hat{w}_{\hat{x}}))_{\hat{x}} - \rho_l \hat{\rho} g \cos \alpha, \quad (5)$$

in the x - and z - directions, respectively. Let us define the shear stress

$$\hat{\sigma} \equiv \hat{\mu} \hat{u}_{\hat{z}}. \quad (6)$$

Then the leading order terms in ϵ of Eq. (4) are

$$-\hat{p}_{\hat{x}} + \hat{\sigma}_{\hat{z}} + \hat{\rho} = 0. \quad (7)$$

Likewise, the leading order terms of (5) are

$$-\hat{p}_{\hat{z}} = 0, \quad (8)$$

which, together with boundary condition (3b) yields $\hat{p}(\hat{x}, \hat{y}, \hat{z}) = \hat{p}_0 - \frac{\gamma_0}{P} \kappa$, where $\hat{p}_0 = \frac{P_0}{P}$. As a consequence,

$$\hat{p}_{\hat{x}} = -\frac{\gamma_0}{P} \kappa_{\hat{x}}. \quad (9)$$

Since (9) and $\kappa \approx h_{xx}$ to leading order in ϵ , we have

$$\hat{p}_{\hat{x}} = -\frac{\gamma_0}{P} \kappa_{\hat{x}} = -\frac{\gamma_0 H^3}{\mu_l U L^3} \left(\hat{h}_{\hat{x}\hat{x}} \right)_{\hat{x}} = -\frac{\epsilon^3}{\text{Ca}} \hat{h}_{\hat{x}\hat{x}\hat{x}} = -\beta \hat{h}_{\hat{x}\hat{x}\hat{x}} \quad (10)$$

where $\beta \equiv \epsilon^3 / \text{Ca}$ and $\text{Ca} = \frac{\mu_l U}{\gamma_0}$ is the capillary number which measures the relative importance between viscous and surface tension forces. Grouping the information in (7)–(10), we have

$$\hat{\sigma}_{\hat{z}} = -\beta \hat{h}_{\hat{x}\hat{x}\hat{x}} - \hat{\rho}. \quad (11)$$

Now we non-dimensionalize the particle equation (2). Following the approach in [21], we adopt the scalings for particle fluxes J_1 and J_3 as

$$[J_1] = \epsilon[J_3], \quad [J_3] = \frac{d^2 U}{H^2},$$

where d is the diameter of the particles. Here $J_1, J_2 \propto d^2$ is due to the diffusive flux approach (the explicit form will be given in the next section) and the ϵ factor in $[J_1]$ is due to the equilibrium requirement in the next section. The non-dimensionalized fluxes are then $\hat{J}_1 = \frac{J_1}{[J_1]}$ and $\hat{J}_3 = \frac{J_3}{[J_3]}$. To leading order, Eq. (2) reduces to $(\hat{J}_3)_{\hat{z}} = 0$, which along with the zero-flux boundary condition leads to

$$\hat{J}_3 = 0, \quad (12)$$

i.e. the particles are in equilibrium in the z -direction. According to the theory for shear-induced migration, the flux \hat{J}_3 depends on the particle concentration ϕ , the shear rate $\dot{\gamma} \approx |\hat{u}_{\hat{z}}|$ and their gradients $\nabla\phi$ and $\nabla\gamma$. Then (12) and (7) form a pair of ODEs for $\hat{\sigma}$ and ϕ that can be used to obtain the particle distribution and velocity \hat{u} at each point \hat{x} . This allows us to integrate out the z -dependence in the model and greatly simplify the equations. For this reason, we define $\phi_0(\hat{x}, \hat{t})$ to be the z -averaged particle concentration, i.e.,

$$\phi_0(x, t) = \frac{1}{h} \int_0^h \phi(x, z', t) dz'. \quad (13)$$

Proceeding with the derivation, we integrate the incompressibility condition (1a), using the kinematic boundary condition $\partial_{\hat{t}} \hat{h} = \hat{w} - \hat{u} \partial_{\hat{x}} \hat{h}|_{\hat{z}=\hat{h}}$ along with the no penetration boundary condition $\hat{w}(0) = 0$ the following evolution equations for \hat{h} :

$$\hat{h}_{\hat{t}} + \left(\int_0^{\hat{h}} \hat{u} d\hat{z} \right)_{\hat{x}} = 0. \quad (14)$$

Indeed,

$$\partial_{\hat{x}} \int_0^{\hat{h}} \hat{u} d\hat{z} = \hat{h}_{\hat{x}} \hat{u}(\hat{h}) + \int_0^{\hat{h}} \partial_{\hat{x}} \hat{u} d\hat{z} = \hat{h}_{\hat{x}} \hat{u}(\hat{h}) - \int_0^{\hat{h}} \partial_{\hat{x}} \hat{w} d\hat{z} = \hat{w}(\hat{h}) - \partial_{\hat{t}} \hat{h} - \hat{w}(\hat{h}).$$

The particle transport equation (2), to next order after the leading balance (12), is simply

$$\partial_{\hat{t}} \phi + \partial_{\hat{x}} (\hat{u} \phi) = 0.$$

Integrating this equation from $\hat{z} = 0$ to $\hat{z} = \hat{h}$ and applying the same boundary conditions as above we have

$$(\hat{h} \phi_0)_{\hat{t}} + \left(\int_0^{\hat{h}} \hat{u} \phi d\hat{z} \right)_{\hat{x}} = 0.$$

To further simplify the model, we further rescale our variables as

$$s = \frac{\hat{z}}{\hat{h}}, \quad \tilde{\sigma}(\hat{t}, \hat{x}; s) = \frac{\hat{\sigma}(\hat{t}, \hat{x}; \hat{z})}{\hat{h}(\hat{t}, \hat{x})}, \quad \tilde{u}(\hat{t}, \hat{x}; s) = \frac{\hat{u}(\hat{t}, \hat{x}; \hat{z})}{\hat{h}^2(\hat{t}, \hat{x})}, \quad \tilde{\phi}(\hat{t}, \hat{x}; s) = \phi(\hat{t}, \hat{x}; \hat{z}).$$

The evolution equations now take the form

$$\hat{h}_{\hat{t}} + \left(\hat{h}^3 \int_0^1 \tilde{u} ds \right)_{\hat{x}} = 0, \quad (\hat{h} \phi_0)_{\hat{t}} + \left(\hat{h}^3 \int_0^1 \tilde{u} \tilde{\phi} ds \right)_{\hat{x}} = 0. \quad (15)$$

Our goal now is to write the integrals in terms of functions only of ϕ_0 and the pressure gradient $\hat{p}_{\hat{x}}$, thus completely eliminating the explicit dependence on \hat{z} . Following a similar approach to the one discussed [21],

we do so by rewriting (15) in terms of integrals relating to the equilibrium distribution $\tilde{\phi}$. In view of Eq. (7) and the boundary condition $\tilde{\sigma}(1) = 0$, we have

$$\tilde{\sigma}(s) = (s-1)\hat{p}_{\hat{x}} + \int_s^1 (1 + \rho_s \tilde{\phi}) ds', \quad (16)$$

which combined with (6) gives

$$\tilde{u}(s) = \int_0^s \frac{\sigma}{\mu(\tilde{\phi})} ds'. \quad (17)$$

Now define functions I, I_1 (omitting the implied dependence on ϕ_0 and $\hat{p}_{\hat{x}}$) by

$$I(s) \equiv \int_0^s \frac{1}{\mu(\tilde{\phi})} \int_{s'}^1 (1 + \rho_s \tilde{\phi}) ds'' ds', \quad (18)$$

$$I_1(s) \equiv \int_0^s \frac{(1-s')}{\mu(\tilde{\phi})} ds', \quad (19)$$

then $\tilde{u}(s) = I(s) - I_1(s)\hat{p}_{\hat{x}}$. Integrating (17) and using the boundary conditions (3), the fluxes in (15) become

$$\int_0^1 \tilde{u} ds = -\hat{p}_{\hat{x}} f_1 + f, \quad \int_0^1 \tilde{\phi} \tilde{u} ds = -\hat{p}_{\hat{x}} g_1 + g,$$

where f, f_1, g and g_1 are given by

$$f \equiv \int_0^1 I(s) ds, \quad f_1 \equiv \int_0^1 I_1(s) ds, \quad g \equiv \int_0^1 \tilde{\phi} I(s) ds, \quad g_1 \equiv \int_0^1 \tilde{\phi} I_1(s) ds. \quad (20)$$

As a result, the equations in (15) become:

$$\hat{h}_{\hat{t}} + \left\{ \hat{h}^3 [-f_1 \hat{p}_{\hat{x}} + f] \right\}_{\hat{x}} = 0, \quad (\hat{h}\phi_0)_{\hat{t}} + \left\{ \hat{h}^3 [-g_1 \hat{p}_{\hat{x}} + g] \right\}_{\hat{x}} = 0,$$

where $\hat{p}_{\hat{x}}$ comes from (10). As we show below, the equilibrium distribution $\tilde{\phi}$ and velocity \tilde{u} can be parametrized by ϕ_0 and $p_{\hat{x}}$; it then follows that the fluxes f, f_1, g, g_1 are functions of ϕ_0 and $\hat{p}_{\hat{x}}$ only. In addition, note that the fluxes are each non-negative. This puts the system in a form suitable for analysis, analogous to the thin film equation without particles or with surface particles (e.g. [11]), but with fluxes that depend in a non-linear fashion on $\hat{p}_{\hat{x}}$. Now that the governing equations have been determined, it remains only to obtain $\tilde{\phi}$ from the equilibrium model.

B. Equilibrium solution

To close the model, we follow [21] and choose a particle flux based on the ‘diffusive flux model’ that describes the balance between the competing effects of sedimentation and shear-induced migration in the normal direction. The expression is

$$J_3 = -\frac{d^2}{4} \left[K_c \phi \partial_z (\dot{\gamma} \phi) + \frac{K_v \phi^2 \dot{\gamma}}{\mu(\phi)} \frac{d\mu(\phi)}{d\phi} \partial_z \phi \right] + \frac{d^2 (\rho_p - \rho_l)(1 - \phi)}{18\mu(\phi)} \phi g \cos \alpha.$$

In the simple geometry of thin-film flow down an incline, the model has been found to be effective in capturing the qualitative behavior of such flows [20, 21] while being simple enough to reduce in the lubrication limit to evolution equations of a typical form for thin films. We remark that more complicated models can be derived through a more rigorous framework (e.g. the suspension balance model [22] or other approaches [1]); the differences between the equations and behavior between the models would be of interest for future work.

With this flux, the dimensionless form in (12) then reads

$$K_c \phi \partial_{\hat{z}} (\hat{\gamma} \phi) + K_v \phi^2 \hat{\gamma} \frac{2}{\phi_m - \phi} \partial_{\hat{z}} \phi - \frac{2\rho_s(1-\phi)\phi}{9\hat{\mu}(\phi)} \cot \alpha = 0, \quad (21)$$

where we have made use of the dimensionless effective viscosity $\hat{\mu}(\phi) = \left(1 - \frac{\phi}{\phi_m}\right)^{-2}$. The shear rate $\hat{\gamma}$ is $\hat{\gamma} = \frac{1}{4} \|\nabla \mathbf{u} + \nabla \mathbf{u}^T\|_{\mathcal{F}} = |\hat{u}_{\hat{z}}|$ to leading order in ϵ . Eq. (21) then becomes an equation for the shear stress $\hat{\sigma} = \hat{\mu}(\phi) \hat{u}_{\hat{z}}$ given by

$$\phi |\hat{\sigma}|_{\hat{z}} + \left(1 + C_1 \frac{\phi}{\phi_m - \phi}\right) |\hat{\sigma}| \phi_{\hat{z}} + C_2(1 - \phi) = 0, \quad (22)$$

where $C_1 = \frac{2(K_v - K_c)}{K_c}$ and $C_2 = \frac{2\rho_s}{9K_c} \cot \alpha$. Then the dynamics in the z -direction [see Eqs. (7) and (22)] are governed by the pair of ODEs

$$\hat{\sigma}_{\hat{z}} = \hat{p}_{\hat{x}} - \hat{\rho}(\phi), \quad \phi_{\hat{z}} = \frac{C_2(\phi - 1) - \phi |\hat{\sigma}|_{\hat{z}}}{|\hat{\sigma}| \left(1 + C_1 \frac{\phi}{\phi_m - \phi}\right)}.$$

In the rescaled variables, these equations become

$$\tilde{\sigma}_s = \hat{p}_{\hat{x}} - (1 + \rho_s \tilde{\phi}), \quad \tilde{\phi}_s = \frac{C_2(\tilde{\phi} - 1) - \tilde{\phi} |\tilde{\sigma}|_s}{|\tilde{\sigma}| \left(1 + C_1 \frac{\tilde{\phi}}{\phi_m - \tilde{\phi}}\right)},$$

subject to the boundary conditions $\tilde{\sigma}(1) = 0$ and $\phi_0 = \int_0^1 \tilde{\phi}(s) ds$. The solution of this system, and consequently the fluxes in (14), are now parametrized by both the averaged volume fraction ϕ_0 and the pressure gradient $\hat{p}_{\hat{x}}$. Note that Eqs. (25) and (26) represent a coupled system of ODEs which, as previously mentioned, may be solved to obtain profiles of \hat{u} and ϕ in the normal direction. In turn, this gives the fluxes needed in the evolution equations (23) and (24) at each point in the axial direction \hat{x} .

To summarize, we first drop the hats and tilde for brevity as we only work with dimensionless system from here on. Our dynamic model is then

$$h_t + \{h^3 [-f_1 p_x + f]\}_x = 0, \quad (23)$$

$$(h\phi_0)_t + \{h^3 [-g_1 p_x + g]\}_x = 0, \quad (24)$$

where the fluxes depend on $\phi(x, t; s)$ and $u(x, t; s)$ through Eqs. (18)–(20). From the equilibrium theory above, $\phi(x, t; s)$ and $u(x, t; s)$ are solutions to the ODE system

$$\sigma_s = p_x - (1 + \rho_s \phi), \quad \sigma(s = 1) = 0, \quad (25)$$

$$\phi_s = \frac{C_2(\phi - 1) - \phi |\sigma|_s}{|\sigma| \left(1 + C_1 \frac{\phi}{\phi_m - \phi}\right)}, \quad \phi_0(x, t) = \int_0^1 \phi(x, t; s) ds, \quad (26)$$

$$u_s = \frac{\sigma}{\mu}, \quad u(0) = 0,$$

and thus can be parameterized by the depth averaged concentration $\phi_0(x, t)$ in (13) and pressure gradient $p_x = -\beta h_{xxx}$, i.e.,

$$\phi(x, t; s) = \phi(s, \phi_0, p_x), \quad u(x, t; s) = u(s, \phi_0, p_x).$$

The equilibrium system (25)–(26) is important in determining the regime in which the model resides: settled or ridged. Therefore, we show the relationship of ϕ , σ and u with the rescaled normal variable s for different values of p_x , parametrized by ϕ_0 , in Figs. 2–5. As p_x and ϕ_0 are varied, the shear rate varies which results in changes in the velocity profile and, consequently, the particle fluid flow dynamics. We show here five types of distinct behavior observed with varying p_x and ϕ_0 , summarized in the phase plane of Fig. 6.

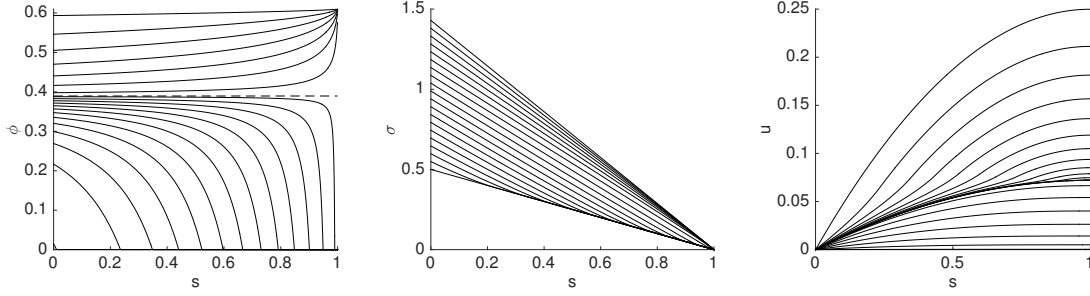


Figure 2: Variation of particle concentration ϕ , shear stress σ , and velocity u in the normal z -direction with $\alpha = 50$ deg for fixed $\hat{p}_{\hat{x}} = 4$ and varying ϕ_0 . In this case, the shear stress is positive and there exists a critical concentration $\phi_c \in (0, \phi_m)$ that separates the settled regime from ridged regime.

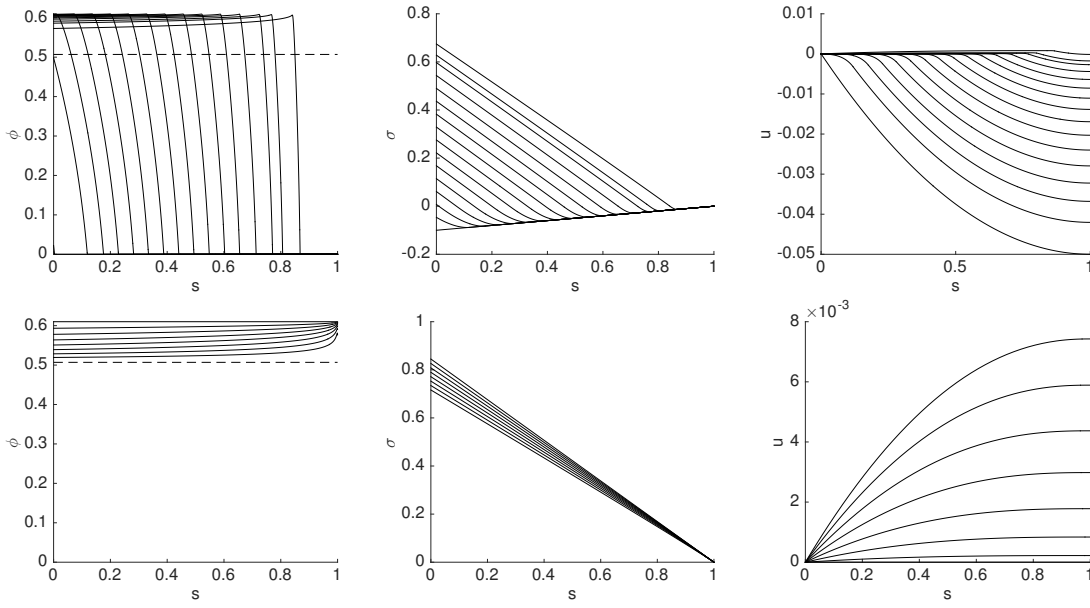


Figure 3: Variation of particle concentration ϕ , shear stress σ , and velocity u in the normal z -direction with $\alpha = 50$ deg for fixed $\hat{p}_{\hat{x}} = 1.1$. In this case, the shear stress changes sign from positive to negative in $0 < s < 1$ for settled regime. Top row: $\phi_0 < \phi_c$ (settled). Bottom row: $\phi_0 > \phi_c$ (ridged).

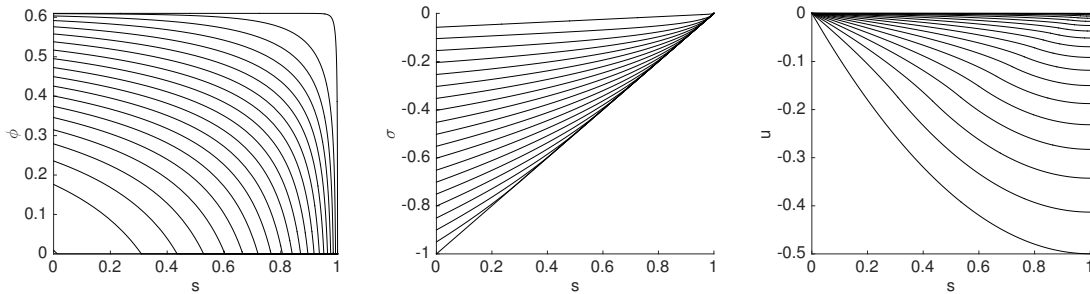


Figure 4: Variation of particle concentration ϕ , shear stress σ , and velocity u in the normal z -direction with $\alpha = 50$ deg for fixed $\hat{p}_{\hat{x}} = 2$ and varying ϕ_0 . In this case, the critical concentration $\phi_c > \phi_m$ and thus the solutions are always settled.

As in the absence of surface tension [21], there exists for some parameter values a critical value $\phi_c(p_x)$ such

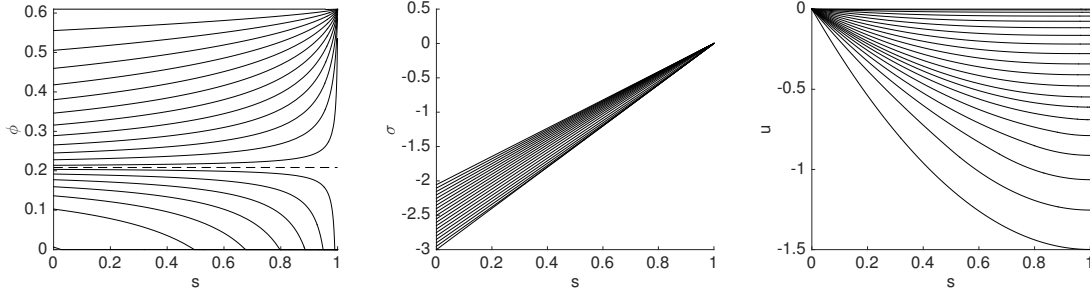


Figure 5: Variation of particle concentration ϕ , shear stress σ , and velocity u in the normal z -direction with $\alpha = 50$ deg for fixed $\hat{p}_x = 4$ and varying ϕ_0 . In this case, the shear stress is negative and there exists a critical concentration $\phi_c \in (0, \phi_m)$ that separates the settled regime from ridged regime.

that $\phi' = 0$ in (26). If σ is single signed then, as shown in [27], the concentration profile $\phi(s)$ is increasing when $\phi_0 > \phi_c$ (particles accumulate at the surface) and decreasing when $\phi_0 < \phi_c$ (particles settle towards the substrate with a clear fluid layer above). If $p_x \leq 1$, then $\sigma \geq 0$ so solutions are monotonic and the velocity profile $u(s)$ is positive (shown in Fig. 2 and corresponding to regions R, S in the phase plane in Fig. 6). If $p_x \geq 1 + \rho_s \phi_0$ then $\sigma \leq 0$ and the velocity is negative (Fig. 5). The critical value ϕ_c lies above ϕ_m when $|p_x - 1 - \rho_s \phi_m| \leq c_2(1 - 1/\phi_m)$, in which case solutions are always settled (Fig. 4) with negative velocity.

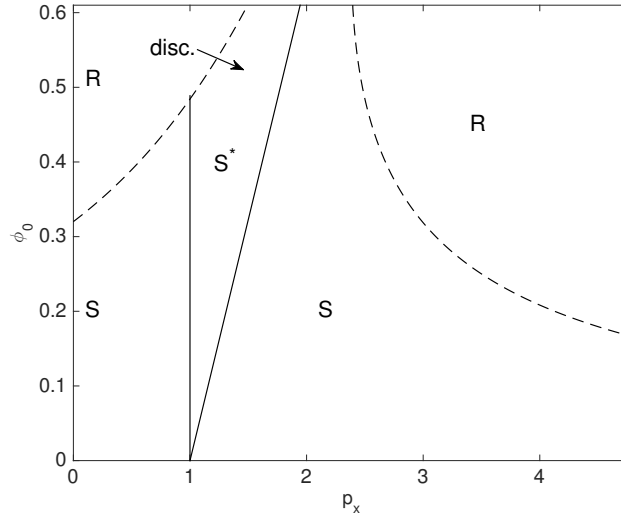


Figure 6: Phase plane at $\alpha = 50$ deg indicating types of solutions of Eqs. (25) and (26) for a given average concentration ϕ_0 and pressure gradient p_x . The dashed curve is the critical concentration $\phi_c(p_x)$; the solid curves are the straight lines $p_x = 1$ and $p_x = 1 + \rho_s \phi_0$. Solution profiles vary discontinuously across the marked segment and otherwise vary continuously with ϕ_0 and p_x . Regions R, S and S^* correspond respectively to ridged, monotonic settled, and non-monotonic settled solutions where σ changes sign.

The behavior in the region $1 \leq p_x \leq 1 + \rho_s \phi_0$ is more complicated. Unlike in the case of no surface tension, the shear changes sign from positive to negative in $0 < s < 1$ for settled solutions (S^* in the phase plane; shown in top row of Fig. 3). This is similar to what happens in the so-called return flows [25]. Particles accumulate to ϕ_m at the point where $\sigma = 0$, now in the interior of the domain, rather than at the surface. For $\phi_0 > \phi_c$ solutions are ridged and monotonic (bottom row of Fig. 3). For numerical convenience (as done in [23]), we introduce a small regularization to the shear stress, $|\sigma| \rightarrow \sqrt{\sigma^2 + \epsilon^2}$ in Eq. (26); this has the effect of preventing ϕ from reaching ϕ_m exactly (which is potentially unphysical) but does not affect the results that follow. The additional ϵ can be interpreted as a correction to the stress accounting for finite particle size. We note that the particle profiles vary discontinuously across the critical

concentration (dashed part of the line in Fig. 6) as they transition from ‘settled’ to ‘ridged’. This is likely an artifact of the equilibrium assumption, which effectively assumes particles to equilibrate instantaneously. The discontinuity, however, only occurs in a small range of p_x and does not appear to be significant.

III. DILUTE APPROXIMATION

In this section, we consider a special case—the dilute approximation, where the fluxes have a closed form. Hereafter, we work only with the non-dimensionalized system and drop hats for brevity. As shown in the end of this section, the equation for the fluid flow is exactly the same as clear fluid, whereas the equation for particle transport depends on the flow free surface in a nonlinear fashion. This simpler case will allow us to better understand how the surface tension modifies the system.

Consider an asymptotic expansion of ϕ : $\phi = 0 + \delta\phi_1 + \delta^2\phi_2 + \dots$ with $\delta \ll 1$. Then the leading order terms of the z -component of the Stokes equations (23) in δ are

$$\frac{d\sigma}{dz} = p_x - 1, \quad (27)$$

recalling $p_x = -\beta h_{xxx}$ from (10). Equation (27) is integrated with respect to z , yielding

$$\sigma(z) = (p_x - 1)(z - h), \quad (28)$$

where we have used $\sigma(h) = 0$. Linearization of the particle transport equation in (23) yields,

$$|\sigma| \frac{d\phi}{dz} = -B, \quad (29)$$

where $B = 2\rho_s \cot \alpha / (9K_c)$. Using Eq. (28) in (29) and, upon integration with respect to z ,

$$\phi(z) = \begin{cases} \frac{B(T-z)}{|1-p_x|h} & 0 < z < T, \\ 0 & T < z < h, \end{cases}$$

where $0 < z < T$ defines the region with particles. Therefore, the z -averaged particle volume fraction is obtained as,

$$\phi_0 = \frac{1}{h} \int_0^h \phi(z) dz = \frac{BT^2}{2|1-p_x|h^2}. \quad (30)$$

Since the linearization of μ about $\phi = 0$ gives $\mu = 1$, the velocity profile via (6) satisfies

$$\frac{du}{dz} = (p_x - 1)(z - h).$$

which, upon integration and application of the no-slip condition at $z = 0$, gives:

$$u(z) = (p_x - 1) \left(\frac{z^2}{2} - hz \right).$$

The spatiotemporal evolution equations (14) form a 2×2 system, defined as,

$$h_t + F_x = 0, \quad (h\phi_0)_t + G_x = 0.$$

The fluxes, F and G are defined as:

$$F = \int_0^h u(z) dz, \quad G = \int_0^T \phi(z) u(z) dz.$$

It is simple enough to see that $F = \frac{1}{3}(1 - p_x)h^3$. Now, for G , integrating across the film, gives

$$G = B \left(\frac{T^3}{6} - \frac{T^4}{24h} \right) \frac{1 - p_x}{|1 - p_x|}.$$

By making use of Eq. (30) and ignoring terms of $\mathcal{O}(\phi_0^2)$, we obtain the following relationship for G :

$$G = \sqrt{\frac{2}{9B}} \phi_0^{3/2} |1 - p_x|^{3/2} h^3 \frac{1 - p_x}{|1 - p_x|}.$$

Substituting the full form of the fluxes in Eqs. (III), we get

$$h_t + \left(\frac{h^3}{3} + \beta h^3 h_{xxx} \right)_x = 0, \quad (31)$$

$$n_t + \sqrt{\frac{2}{9B}} \left(\phi_0^{3/2} |1 - p_x|^{1/2} (1 - p_x) h^3 \right)_x = 0, \quad (32)$$

where $n = h\phi_0$ and we have made use of $p_x = -\beta h_{xxx}$. We observe from Eqs. (31) and (32) that the particle dynamics decouple from the fluid motion. Note that Eq. (31) describes the dynamics of the clear, thin-film fluid. Setting $\beta = 0$ recovers the simple model [21] which ignores effects due to surface tension. We note that in the absence of surface tension effects, the system of Eqs. (31), (32) may be solved exactly. In the presence of surface tension ($\beta \neq 0$) with positive initial conditions, (31) is expected to have a smooth solution (see [3]) and (32) becomes a scalar conservation law that can be solved exactly.

IV. NUMERICAL SCHEME

In this section, we explain in detail the numerical scheme for solving the system (23) (24). Recalling the definition of p_x in (10), the system reads (omitting hats)

$$h_t + (h^3 f)_x = -\beta (h^3 f_1 h_{xxx})_x, \quad (33)$$

$$(h\phi_0)_t + (h^3 g)_x = -\beta (h^3 g_1 h_{xxx})_x. \quad (34)$$

Note that fluxes $f(\phi_0, p_x)$ and $g(\phi_0, p_x)$ depend on p_x , thus the left hand side of (33) (34) is no longer a simple hyperbolic system, which makes its discretization ambiguous. To overcome this difficulty, we rewrite the system (33) and (34) as

$$h_t + (h^3 f(\phi_0, 0))_x = -\beta (h^3 \tilde{f}_1 h_{xxx})_x \quad (35)$$

$$(h\phi_0)_t + (h^3 g(\phi_0, 0))_x = -\beta (h^3 \tilde{g}_1 h_{xxx})_x \quad (36)$$

where

$$\tilde{f}_1 = f_1 - \frac{f(\phi_0, 0) - f(\phi_0, p_x)}{p_x}, \quad \tilde{g}_1 = g_1 - \frac{g(\phi_0, 0) - g(\phi_0, p_x)}{p_x}.$$

Then the left hand side of (35) (36) reduces to the original model without surface tension, which has been shown to be hyperbolic [27]. The modified fluxes \tilde{f}_1 and \tilde{g}_1 are well-defined and bounded as $p_x \rightarrow 0$ due to the linear dependence of the equilibrium equation (25) on p_x . In addition, these fluxes remain non-negative. The main difficulty comes from the fourth order diffusion, for which an explicit treatment poses a constraint on time step $\Delta t \sim \Delta x^4$, whereas implicit treatment necessitates inversion of a nonlinear system. We propose here a semi-implicit discretization with an explicit discretization of the nonlinear fluxes \tilde{f}_1 and \tilde{g}_1 and implicit for the linear fourth order diffusion. The complicated form of the flux functions and potential lack of smoothness motivates the choice of a semi-implicit method preferable in which these fluxes are treated explicitly.

More precisely, let Δx be the mesh size and Δt^k be the adaptive time step at k th step. Denote $h_j^k = h(x_j, t^k)$, $(f_i)_j^k = f_i(x_j, t^k)$, and $(\phi_0)_j^k = \phi_0(x_j, t^k)$, where $x_j = j\Delta x$ and $t^k = \sum_{l=0}^{k-1} \Delta t^l$. First, we discretize the fluid flow (35) as

$$\begin{aligned} \frac{h_j^{k+1} - h_j^k}{\Delta t^k} + \frac{(h^3 f(\phi_0, 0))_j^k - (h^3 f(\phi_0, 0))_{j-1}^k}{\Delta x} = & -\frac{\beta}{\Delta x^4} \left\{ \frac{(h^3 \tilde{f}_1)_j^k + (h^3 \tilde{f}_1)_{j+1}^k}{2} (h_{j+2}^{k+1} - 3h_{j+1}^{k+1} + 3h_j^{k+1} - h_{j-1}^{k+1}) \right. \\ & \left. - \frac{(h^3 \tilde{f}_1)_j^k + (h^3 \tilde{f}_1)_{j-1}^k}{2} (h_{j+1}^{k+1} - 3h_j^{k+1} + 3h_{j-1}^{k+1} - h_{j-2}^{k+1}) \right\}. \end{aligned} \quad (37)$$

and we use upwind difference for the transport part as the direction of the flow is downward. The fluxes f_i depend on $(\phi_0)_j^k = \frac{n_j^k}{h_j^k}$ and

$$(p_x)_j^k = -\beta(h_{xxx})_j^k = -\beta \frac{h_{j+2}^k - 2h_{j+1}^k + 2h_{j-1}^k - h_{j-2}^k}{2\Delta x^3}.$$

Δx is the spatial grid and we choose it uniformly for simplicity; it can be directly generalized to nonuniform mesh if we want to refine the resolution at the wave front. The time step Δt is chosen adaptively according to some stability condition. In all the examples that follow, we consider Dirichlet boundary condition for both boundaries and thus we simply set the value of h to be the boundary data near the boundary.

Next, for the particle transport (36), although the fourth order diffusion is in h not in n , it cannot be considered as part of the flux or the source as it may render the scheme unstable. Instead, we should discretize $\beta(h^3 \tilde{g}_1 h_{xxx})_x$ in the same way as $\beta(h^3 \tilde{f}_1 h_{xxx})_x$ in (35). More precisely, the scheme for (34) reads

$$\begin{aligned} \frac{n_j^{k+1} - n_j^k}{\Delta t^k} + \frac{(h^3 g(\phi_0, 0))_j^k - (h^3 g(\phi_0, 0))_{j-1}^k}{\Delta x} = & -\frac{\beta}{\Delta x^4} \left\{ \frac{(h^3 \tilde{g}_1)_j^k + (h^3 \tilde{g}_1)_{j+1}^k}{2} (h_{j+2}^{k+1} - 3h_{j+1}^{k+1} + 3h_j^{k+1} - h_{j-1}^{k+1}) \right. \\ & \left. - \frac{(h^3 \tilde{g}_1)_j^k + (h^3 \tilde{g}_1)_{j-1}^k}{2} (h_{j+1}^{k+1} - 3h_j^{k+1} + 3h_{j-1}^{k+1} - h_{j-2}^{k+1}) \right\}. \end{aligned} \quad (38)$$

Without particles, the numerical method reduces to a straightforward semi-implicit method for the well-studied thin film equation $h_t + (h^3)_x = -(h^3 h_{xxx})_x$ that is stable [31]. The approach has also been studied more generally in more recent work [4]. For suspension flow, a semi-implicit method was used to simulate a coupled system with simpler flux functions and studied numerically [10, 16]. A small diffusion term arising from shear-induced migration was included to improve numerical stability. Similar systems that arise in surfactant spreading have been solved using this approach [11] and using finite element methods with rigorously established convergence properties [12]. The model here, in contrast, lacks a natural diffusion term for the particle phase and, crucially, the flux functions degenerate at the maximum packing fraction.

As noticed in [27], one of the most important properties of the solution to the original hyperbolic system (the one without surface tension) is that $\phi_0(t, x) = \frac{n(t, x)}{h(t, x)}$ stays in the interval $[0, \phi_m]$, even in the case of a singular shock. In what follows, we will show the reason for it and then explains how it inspires the discretization (38). First we have the following lemma.

Lemma 1. *The flux pairs $(f_1(\phi_0), g_1(\phi_0))$ and $(f(\phi_0), g(\phi_0))$ are non-negative and satisfy $g(\phi_0) \leq \phi_m f(\phi_0)$.*

Proof. Since we always choose the physical solution to the equilibrium system (25)(26) such that $0 \leq \phi \leq \phi_m$, the averaged value ϕ_0 also falls into the range $[0, \phi_m]$. Since $I(s)$ in (18) is non-negative, from the definition of the fluxes in (20) we have

$$g(\phi_0) = \int_0^1 \phi(s) I(s) ds \leq \phi_m \int_0^1 I(s) ds = \phi_m f(\phi_0).$$

Similarly, $I_1(s)$ in (19) is non-negative and so $g_1(\phi_0) \leq \phi_m f_1(\phi_0)$. \square

To proceed, we consider a special case when $\beta = 0$, then $p_x \equiv 0$, and the fluxes $f(\phi_0)$ and $g(\phi_0)$ reduce to the original flux in [21] without surface tension, and the system (33)(34) reduces to the conservation laws where a simple upwind difference scheme suffices to give the correct solution. For such a system, we have the following property.

Theorem 2. *If the time step Δt^k satisfies the CFL condition*

$$\frac{\Delta t^k}{\Delta x} \leq \min_j \left\{ \frac{1}{h^2 f(\phi_0)}, \frac{\phi_0}{h^2 g(\phi_0)}, \frac{\phi_m - \phi_0}{(\phi_m f(\phi_0) - g(\phi_0))h^2} \right\}_j^k, \quad (39)$$

the the solution to the evolution system (37) (38) with $p_x \equiv 0$ satisfies $0 \leq \phi_0^k = \frac{n_j^k}{h_j^k} \leq \phi_m$.

Proof. Rewrite the upwind scheme in (37) and (38) as

$$n_j^{k+1} = n_j^k - \frac{\Delta t^k}{\Delta x} [(h^3 g)_j^k - (h^3 g)_{j-1}^k], \quad h_j^{k+1} = f_j^k - \frac{\Delta t^k}{\Delta x} [(h^3 f)_j^k - (h^3 f)_{j-1}^k].$$

Then positivity of h_j^{k+1} and n_j^{k+1} is guaranteed if Δt^k satisfies the CFL condition (39), so it is with ϕ_0^{k+1} . Now let us consider the quantity $\phi_m h_j^{k+1} - n_j^{k+1}$. Notice that

$$(\phi_m h - n)_j^{k+1} = (\phi_m h - n)_j^k - \frac{\Delta t^k}{\Delta x} [(h^3 \phi_m f - h^3 g)_j^k - (h^3 \phi_m f - g)_{j-1}^k],$$

thus it is easy to check that if $(\phi_m h - n)_j^k = 0$ at one position x_j and a specific time t^k , $(\phi_m h - n)_j^{k+1} = 0$ thanks to Lemma 1 and the fact $f(\phi_m) = g(\phi_m) = 0$. Now it is left to check that if $(\phi_m h - n)_j^k > 0$ for any x_j and t^k , we have $(\phi_m h - n)_j^{k+1} \geq 0$. This is readily followed by the third algebraic expression in the CFL constraint (39). \square

Remark 3. The first two constraints in the CFL condition (39) are the common conditions to guarantee the positivity of the upwind solution, whereas the third one is an extra requirement to preserve the upper bound of ϕ_0 . However, this extra requirement is not restrictive at all. Indeed, we can check the ratio

$$\frac{\phi_m - \phi_0}{\phi_m f(\phi_0) - g(\phi_0)} \bigg/ \frac{1}{f(\phi_0)} = \frac{(\phi_m - \phi_0)f(\phi_0)}{\phi_m f(\phi_0) - g(\phi_0)}, \quad (40)$$

which is uniformly bounded with an $\mathcal{O}(1)$ upper bound (please see the appendix).

Remark 4. Analytically, for the hyperbolic system without surface tension ($\beta = 0$ in (33) (34)) if initially $h(x, 0) < \phi_m n(x, 0)$ and we assume the solution is sufficiently smooth, then $\phi_0(t, x) < \phi_m$ still holds. This can be seen following the characteristics of the system

$$h_t + (h^3 f(\phi_0))_x = 0, \quad \xi_t + (h^3 \phi_m f(\phi_0) - h^3 g(\phi_0))_x = 0,$$

where $\xi = \phi_m h - n$ and ϕ_0 is recovered via $\phi_0 = \frac{\phi_m h - \xi}{h}$. However, once the shock or rarefaction forms, we need to resort to the Hugoniot locus or integral curve [17, 27] to study the behavior of the solution. Indeed, in the interesting case when there is a singular shock, both h and n increase unboundedly at the wave front of the shock, but $\phi_0 = \frac{n}{h}$ is always bounded by ϕ_m , which is seen from the fact that the Hugoniot locus in the (h, ϕ_0) -plane always stay below $\phi_0 = \phi_m$ (see Fig. 4.1 and Theorem 4.1 in [27]). Therefore, in the case of double/singular shock, the volume concentration $\phi_0(t, x)$ is still bounded above by ϕ_m .

Therefore, in the absence of surface tension, the upper bound of ϕ_0 is preserved both analytically and numerically. Inspired by the above argument, we notice that, in the presence of surface tension, a good choice of discretization of the term $\beta h^3 g_1 h_{xxx}$ in (34) is that it is discretized in the same manner as $\beta h^3 f_1 h_{xxx}$ in (33). However, since the theory of the uniform boundedness in ϕ_0 is still lacking for (34) (33), the rigorous estimate of numerical solution (37) (38) sharing the same property is beyond the scope of this paper, and we leave it to future work.

V. NUMERICAL SIMULATION

In this section, we conduct several numerical simulations to show how the model performs in the presence of surface tension. We first present the results starting from Riemann initial data representing a ‘constant flux’ setting. Motivated by physical experiments carried out on the experimental set-up housed in the Applied Mathematics Department at UCLA, we then investigate the numerical solutions for the ‘constant volume’ case and show some experimental results. All the simulations are carried out at angle of 30 degrees.

In this case, we consider the Dirichlet boundary condition $h(x_L, t) = h_L$, $n(x_L, t) = \phi_I h_L$ for the left boundary and $h(x_R, t) = h_R$, $n(x_R, t) = \phi_I h_R$ for the right boundary.

A. Riemann initial data

Consider Riemann initial data

$$h(0, x) = h_R + \frac{1}{2} (h_L - h_R) (1 - \tanh(10x)), \quad (41)$$

and $n(0, x) = \phi_I h(0, x)$ where ϕ_I is the initial concentration, h_L and h_R are the height in the reservoir and precursor, respectively. Eq. (41) describes a step-like profile for the interfacial height, consistent with investigating slow flows down rectangular planes.

Dilute case

We first give one example for the dilute approximation (31) (32) with $\beta = 1$, the solution of which is compared with the one without surface tension, i.e., $\beta = 0$. Here since the h evolution is decoupled from n evolution, we use a semi-implicit scheme (similar to (37)) for (31) and use a local Lax-Friedrichs scheme for (32). The result is shown in Fig. 7; we observe that the position of the front of the wave is the same in both models with and without surface tension. In the presence of surface tension, it shows that the flow develops a capillary ridge in h , representing a travelling-wave solution which moves with a constant velocity. Such a capillary ridge is subject to spanwise instabilities that give rise to fingering patterns [2, 13, 15], which is an interesting problem for further study.

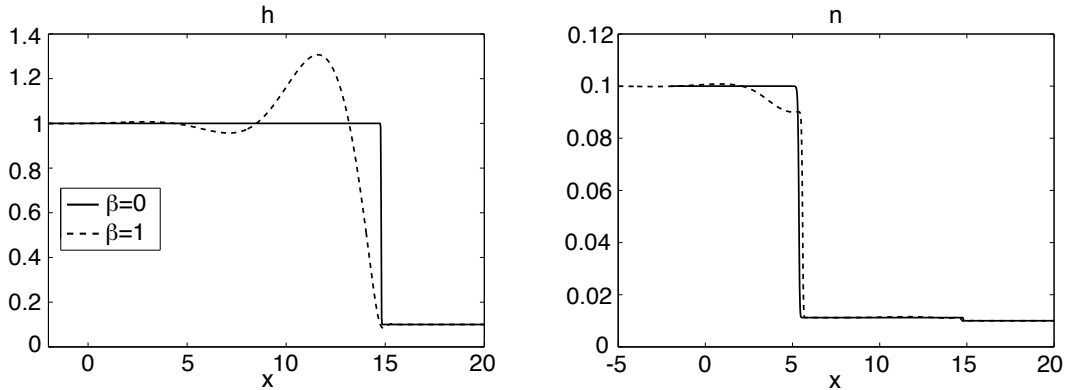


Figure 7: Comparison of the height h and integrated particle density $n = h\phi_0$ for the dilute model with and without surface tension (ST) at time $t = 40$. In the case with surface tension, $\beta = 1$. The rest of the parameters are chosen as: $h_L = 1$, $h_R = 0.1$ and $\phi_I = 0.1$.

Settled case

We now move away from the dilute limit and turn our attention to the full model described by Eqs. (23) and (24). First, we focus on a case where the concentration is low giving rise to the settled flow pattern, which corresponds to a double-shock solution when surface tension is neglected. We consider the following parameters $h_L = 1$, $h_R = 0.1$ and $\phi_I = 0.2$ in all simulations and investigate the effect of surface tension by varying the value of the parameter β . We compare the numerical solutions with $\beta = 0, 10^{-3}, 10^{-2}$ at $t = 15$ in Fig. 8, where stronger surface tension effect results in more pronounced capillary ridge in both shocks. Here, we choose $\Delta x = 0.025$, $\Delta t = 0.01$. We observe that the previous, hyperbolic model captures the location of the front of the flow while surface tension leads to the development of two ridges: a trailing one, representing the particle-concentrated region and a leading ridge, representing the particle-free region. The leading wave forms at the contact line which we expect to be unstable to fingering. From experimental observations, the fingering is more visible at the front of the flow while, at the particle-fluid separation, the fingering appears to be more suppressed.

In Fig. 9, we choose $\beta = 0.1$ corresponding to more distinct surface tension effects, and plot the profiles of h and n at different times, indicating that the solution is composed of two traveling waves. Again, $\Delta x = 0.025$, $\Delta t = 0.01$.

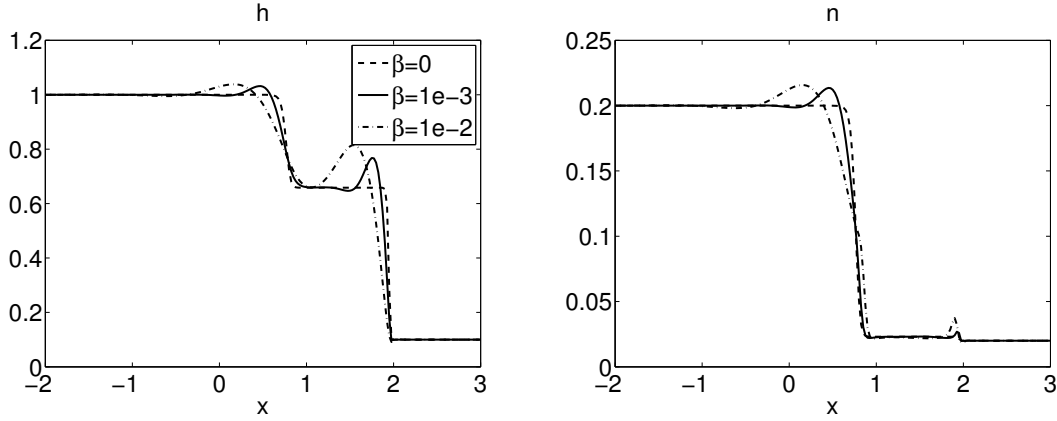


Figure 8: Computation of the full model given by Eqs. (23) and (24) with surface tension for different $\beta = 0, 1e - 3, 1e - 2$ at time $t = 15$. The left panel shows the film height solution and the right panel shows the solution of the product of the height and particle volume concentration. Here, $h_L = 1$, $h_R = 0.1$ and $\phi_I = 0.2$.

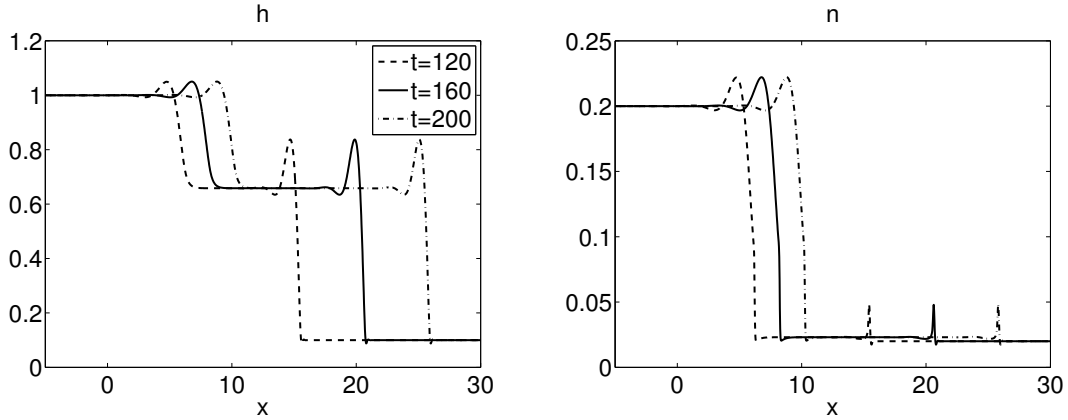


Figure 9: Computation of the full model given by Eqs. (23) and (24) with surface tension for $\beta = 0.1$ at different times. Here $h_L = 1$, $h_R = 0.1$ and $\phi_I = 0.2$.

We now explore the *double-shock* formation in the ridged regime. Consider the initial data (41) but with $h_L = 1$ and $h_R = 0.2$. $\phi_I = 0.5$. As shown in [27], this initial data will produce a double shock with intermediate height and concentration larger than the left and right states. Here we compare our results with $\beta = 0.1$ and without surface tension, i.e., $\beta = 0$. Here, we choose $\Delta x = 0.05$, $\Delta t = 0.01$. The results are gathered in Fig. 10 where the capillary ridge emerges in the second shock near the moving contact line in the presence of surface tension, as one would expect from experimental results.

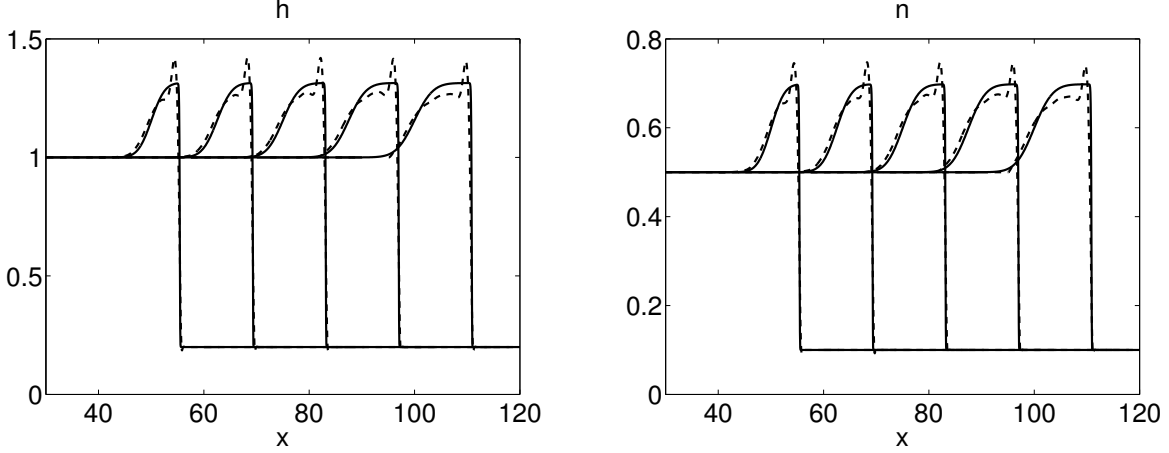


Figure 10: Comparison of $\beta = 0$ and $\beta = 0.1$ for different times $t = 2000, 2500, 3000, 3500$, and 4000 . Blue dashed curve: $\beta = 0$. Black solid curve: $\beta = 0.1$. Here we used a moving mesh with speed $s = 0.0275$ computed from the initial data and reform the results according to the distance it should advance at the above times.

Next, we investigate the singular shock. If we choose $h_L = 1$, $h_R = 0.02$ and $\phi_I = 0.5$, the solution to the original hyperbolic system is a singular shock. Here we first show a comparison of the solution with and without surface tension. The results are collected in Fig. 11 where we display the solutions at different times $t = 400, 800, 1200, 1600$, and 2000 . Here the black solid curve is without surface tension, whose solution in H produces a singularity, while the blue dashed is for $\beta = 0.05$ where the profile in h has been regularized. To further see this, we compare the maximum height of the fluid (h) for model (23) (24) by decreasing the

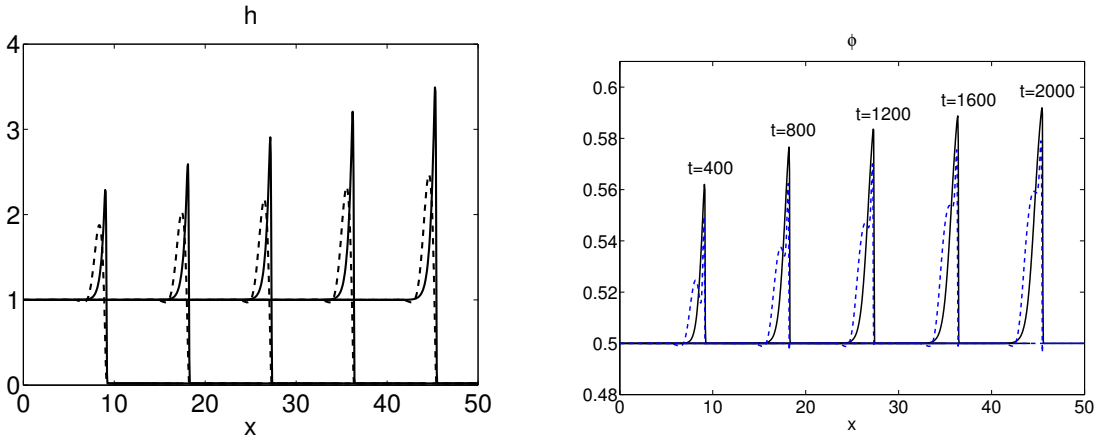


Figure 11: Comparison of no surface tension (i.e., $\beta = 0$, black solid curve) and $\beta = 0.05$ (blue dashed curve) for different times $t = 400, 800, 1200, 1600, 2000$. $\Delta x = 0.05$, $\Delta t = 0.0025$.

mesh size, with $\beta = 0.1$ and $\beta = 0$, respectively. It is observed from Fig. 12 that surface tension ($\beta = 0.1$) successfully suppresses the singular shock, resulting in a particle-rich ridge with uniformly bounded height

for finite time. On the other hand, without surface tension the height does not have a uniform growth when we refine the mesh, indicating the presence of singularity.

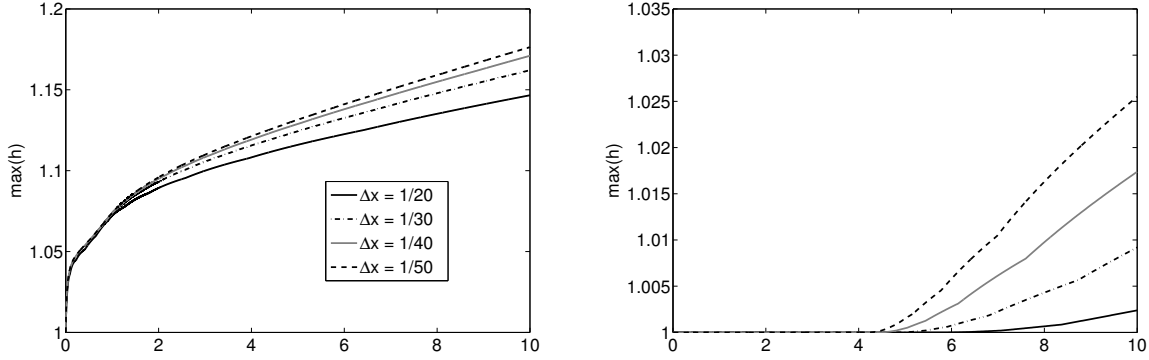


Figure 12: $\max_x h(t, x)$ versus t for different mesh grids for model (23)–(24) with initial condition $h_L = 1$, $h_R = 0.02$ and $\phi_I = 0.5$. Left: $\beta = 0.1$, with surface tension. Right: $\beta = 0$, without surface tension.

B. Conserved volume initial data

In this section, we further demonstrate that the presence of surface tension will not affect the large-scale dynamics but only modify the wave front by using the laboratory parameters from recent experiments [5]. In the experimental data obtained in [5], height profiles for the suspension in the incline problem were obtained by use of a laser sheet, capturing the evolution of the capillary ridge. The suspension used was a viscous oil (PDMS with kinematic viscosity $\nu = 1000$ cSt and surface tension $\gamma = 0.02$ N/m) with 0.2 mm particles and densities $\rho_\ell = 971$ kg/m³ and $\rho_p = 3800$ kg/m³, similar to previous experiments [21].

With these parameters, $\beta = \frac{\epsilon^3}{Ca} = \frac{\gamma H}{L^3 \rho_l g \sin \alpha} = 0.042$. Initial data takes the following form:

$$h(0, x) = \begin{cases} \frac{110 \cdot 0.75}{10 \cdot 14}, & \text{for } -10 \leq x \leq 0 \\ 0.02 * \frac{110 \cdot 0.75}{10 \cdot 14}, & \text{elsewhere} \end{cases}, \quad \phi_0(0, x) = \phi_I, \quad n(0, x) = \phi_I h(0, x), \quad (42)$$

and boundary data are taken be $h(x_L, t) = h(x_R, t) = 0.02 * \frac{110 \cdot 0.75}{10 \cdot 14}$, $n(x_L, t) = n(x_R, t) = \phi_I 0.02 * \frac{110 \cdot 0.75}{10 \cdot 14}$. Figure 13 displays the comparison of solutions to model (23)–(24) with ($\beta = 0.042$, solid curve) and without surface tension ($\beta = 0$, dashed curve).

In Figure 14, we show two typical examples of measured height profiles. Varying the total volume effectively changes the left and right states (as in (42)), thereby allowing for the possibility of detecting the transition between singular and double shocks. In the parameter regime tested, which is restricted by the equilibrium assumption, only a single, sharp ridge evolves (see Figure 14). The height of the ridge increases with angle; for moderate angles, the effect of spreading due to the normal component of gravity (neglected in the model here) is significant (compare the ridges for angles $\alpha = 45$ deg and $\alpha = 55$ deg in Figure 14). Even at large angles, this diffusion dampens the growth of the ridge somewhat but the effect is small for $\alpha = 55$ deg. It is difficult to determine whether the observed ridge corresponds to the singular shock solution (as the model would predict) or a double shock, as the double shock evolves over much longer time period than the current experiments allow. Further experiments may better illuminate the behavior of the fronts (as singular shocks or otherwise) and the particle distribution therein. In addition, in the high concentration regime, non-Newtonian effects (particularly at the front) may be important; this is evident, e.g. as the typical fingering instability evolves and the high-concentration ‘fingers’ will tend to solidify and/or break. The fingering instability also has an effect on the formation of the ridge, which makes quantitative comparison to the one-dimensional model of limited use. Fully studying the physical model therefore requires extending the model to two dimensions, which is beyond the scope of this work.

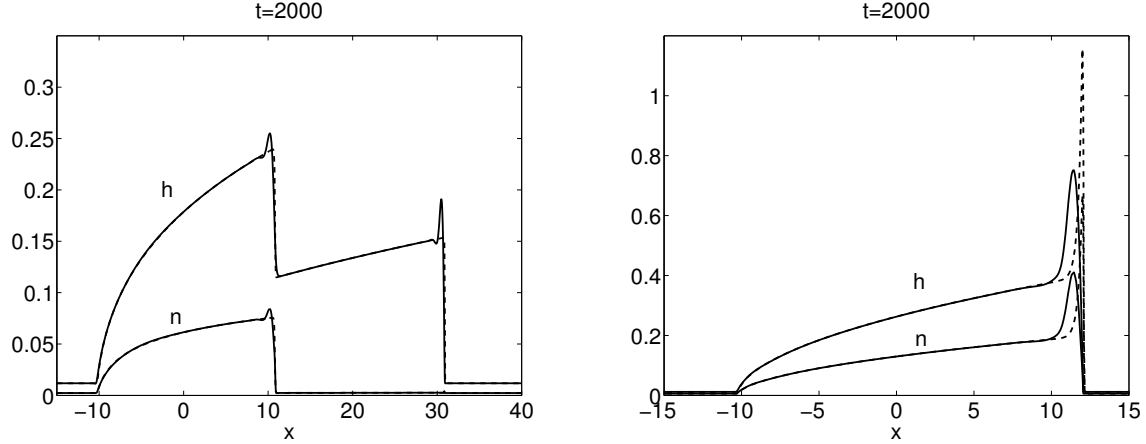


Figure 13: Comparison of no surface tension (i.e., $\beta = 0$, dashed curve) and $\beta = 0.042$ (solid curve) for models with initial data (42). Left: settled case with $\phi_0 = 0.2$. Right: ridged case with $\phi_0 = 0.5$.

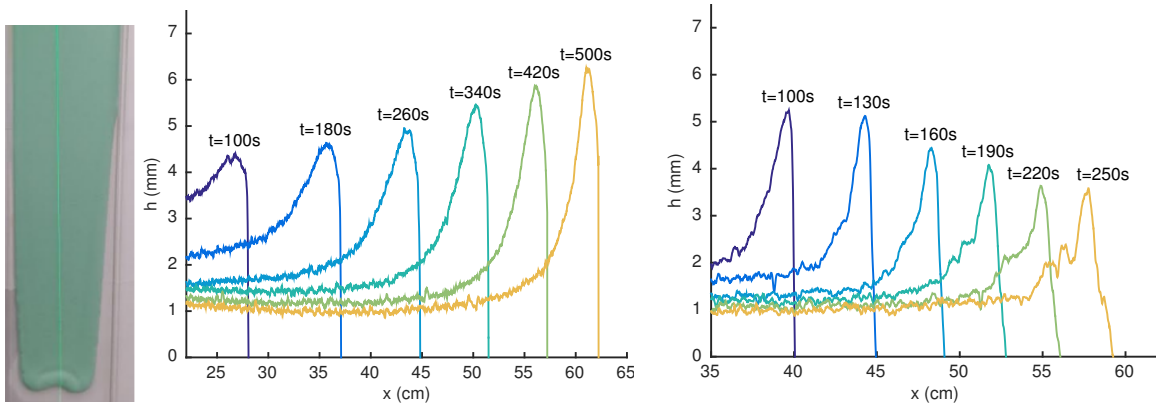


Figure 14: Left/center: An experimental picture and height profile near the front for $\phi_0 = 0.5$ and $\alpha = 55$ deg (the vertical line in the figure is the laser line from which the height profiles are measured). Right: experimental height profile for $\alpha = 45$ deg (right) with an initial volume of 110 ml.

VI. CONCLUDING REMARKS

In this paper, we derive a model for the evolution of a gravity-driven thin film laden with particles in the presence of surface tension effects. This model takes the form of conservation law with a fourth order nonlinear diffusion, the latter arises from capillarity due to the addition of surface tension. We propose a semi-implicit scheme that is able to effectively solve the models without a severe stability constraint. We carry out numerical simulations with system parameters corresponding to three distinct flow regimes observed in experiments. We observe that in the settled case where there exists separation between the particle-rich and particle-free regions the numerical solution is described by two capillary shocks for each region. In the ridged case where the particles accumulate at the front of the flow, in the absence of surface tension effects, the solution is described by a singular shock which is physically unrealistic. The addition of surface tension acts to regularize the thin film height solution thus suppressing the singular shock.

Our study at present of the ridge in the presence of surface tension is primarily numerical; asymptotic or analytical study of the growth of the ridge and the regularizing effect of surface tension would be an interesting direction for future work. On the analysis side, it is very interesting to study the well-posedness of the system (23) (24) (or (35) (36)), which is of a complicated hyperbolic-parabolic type, especially in the case of a singular shock. Similar equations have been studied in modeling of surfactant spreading [11]. These equations are also a fourth-order parabolic equation for the film height coupled to a particle transport

equation which can be solved using semi-implicit methods. Mathematically, the model proposed here have some key differences which complicate the problem. The conserved form of the system is for the film height h and integrated concentration $h\phi$, while the fluxes still depend on the concentration ϕ . As a consequence, a numerical scheme in conserved form must be discretized carefully to ensure that the approximation for ϕ remains appropriately bounded. In addition, the fluxes f, g that drive the bulk fluid motion, which are first-order in the absence of surface tension, gain a complicated non-linear dependence on h_{xxx} . Progress on analysis of the equations may also aid in developing numerical schemes with desirable properties, such as ensuring boundedness of the particle concentration.

This work brings many challenging questions for future study. On the modeling and numerics side, extending the model to two dimensions is necessary in understanding the fingering instability. The simplest generalization to two dimensions is to assume the shear-induced migration flux depends only on the total shear rate $\dot{\gamma} = \sqrt{|\mu u_z|^2 + |\mu v_z|^2}$ where v is the y -velocity (see e.g. [30]). One then obtains a similar equilibrium ODE and fluxes that now depend on both components of the pressure gradient ($\nabla p = -\beta \nabla \Delta h$). The resulting equation is again similar to the thin film equation in two dimensions. However, the typical fingering instabilities that arise and dependence on p_y further exacerbate the numerical difficulties we have discussed in one dimension. In addition, from a physical perspective, it is not clear that the use of the total shear rate is a good approximation, as the behavior of shear-induced migration in more complicated geometries is not as straightforward and may necessitate the use of more complicated models (for example, taking into account the role of anisotropic normal stresses [18, 24]).

Acknowledgements: The authors would like to thank Dirk Peschka and Roman Taranets for fruitful discussions and Sarah Burnett, Jesse Kreger, Hanna Kristensen, and Andrew Stocker for their experimental work. This work is funded by NSF grants DMS-1312543 and DMS-1045536.

VII. APPENDIX

A. Experiments to verify constant surface tension

To justify the assumption that surface tension is constant, we carried out a series of experiments to measure the surface tension of a fixed volume of PDMS with various particle volume concentrations within the range of $0 < \phi < \phi_m$, where ϕ_m represents the maximum packing fraction. The experimental method used for the determination of the surface tension of the slurry sample is known as the pendant drop test. A drop of the slurry sample is suspended by a tube; the resulting shape of the drop is a consequence of increased pressure produced inside the drop as a result of the interfacial tension [26]. The pressure difference is proportional to the changing radii in the pendant-shaped drop while the interfacial tension is the constant of proportionality. We took measurements of surface tension as a function of particle volume concentration and the results are collected in Fig. 15, which shows that the surface tension was found to be constant at about 20 mN/m, the same as the surface tension for the silicon oil without particles.

B. Uniform bound for ratio

Here we show the uniform bound of the ratio (40). First notice that when $\phi_0 \leq \phi_{\text{crit}}$ (ϕ_{crit} is the critical value that distinguishes the ‘settled’ and ‘ridged’ regime [21]), we have $g(\phi_0) \leq \phi_0 f(\phi_0)$ (Theorem 2.2 in [27]), so the ratio is bounded by 1. When $\phi_0 > \phi_{\text{crit}}$, we see that the ratio is an increasing function in ϕ_0 (we can check it numerically, please see Fig. 16), thus it suffices to check its bound near ϕ_m . Consider the following Taylor expansion

$$\begin{aligned} f(\phi_0) &= f(\phi_m) + f'(\phi_m)(\phi_0 - \phi_m) + \frac{1}{2}f''(\phi_m)(\phi_0 - \phi_m)^2 + \frac{1}{3!}f'''(\phi_m)(\phi_0 - \phi_m)^3 + \mathcal{O}((\phi_m - \phi_0)^4), \\ g(\phi_0) &= g(\phi_m) + g'(\phi_m)(\phi_0 - \phi_m) + \frac{1}{2}g''(\phi_m)(\phi_0 - \phi_m)^2 + \frac{1}{3!}g'''(\phi_m)(\phi_0 - \phi_m)^3 + \mathcal{O}((\phi_m - \phi_0)^4). \end{aligned}$$

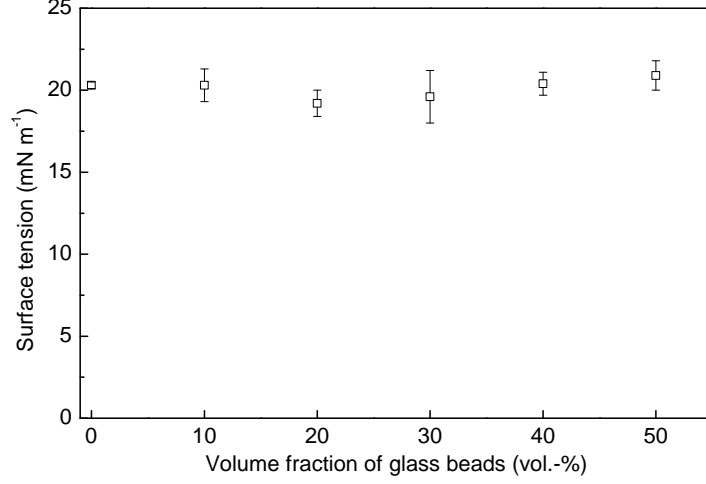


Figure 15: Surface tension γ_0 measured for silicon oil with different concentrations of glass beads.

Since we have $f(\phi_m) = g(\phi_m) = f'(\phi_m) = g'(\phi_m) = 0$ and $\phi_m f''(\phi_m) = g''(\phi_m) \neq 0$ (see Lemma 4.3 in [27]), the ratio (40) expands as

$$\frac{(\phi_m - \phi_0)f(\phi_0)}{\phi_m f(\phi_0) - g(\phi_0)} = \frac{(\phi_m - \phi_0) \left[\frac{1}{2} f''(\phi_m)(\phi_0 - \phi_m)^2 + \frac{1}{3!} f'''(\phi_m)(\phi_0 - \phi_m)^3 + \mathcal{O}((\phi_m - \phi_0)^4) \right]}{\frac{1}{3!} [\phi_m f'''(\phi_m) - g'''(\phi_m)](\phi_0 - \phi_m)^3 + \mathcal{O}((\phi_m - \phi_0)^4)}. \quad (43)$$

Recall again the calculation in [27] that

$$\begin{aligned} f''(\phi_m) &= \int_0^1 \frac{(1 + \rho_s \phi_m)(1 + B)}{\mu_l \phi_m^2} [1 - (1 - s)^{2B+2}] ds, \\ \phi_m f'''(\phi_m) - g'''(\phi_m) &= -3 \int_0^1 \frac{(1 + \rho_s \phi_m)(1 + B)}{\mu_l \phi_m^2} [1 - (1 - s)^{2B+2}] (1 + B)(1 - s)^B ds, \end{aligned}$$

where $B = \frac{\rho_s \phi_m^2 + (C_2 + 1)\phi_m - C_2}{C_1 \phi_m (1 + \rho_s \phi_m)}$, then the ratio (43) is estimated, with higher order term neglected, as $\frac{3(2B+2)}{2(2B+3)}$.

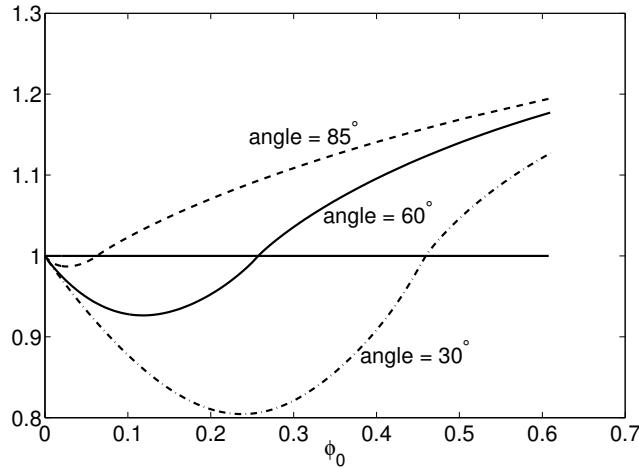


Figure 16: The ratio (40) vs ϕ_0 . The intersections with the horizontal line are ϕ_{crit} at different angles.

-
- [1] Andrew J Archer, Mark J Robbins, and Uwe Thiele. Dynamical density functional theory for the dewetting of evaporating thin films of nanoparticle suspensions exhibiting pattern formation. *Physical Review E*, 81(2):021602, 2010.
 - [2] A. L. Bertozzi and M. Brenner. Linear stability and transient growth in driven contact lines. *Phys. Fluids*, 9:530–539, 1997.
 - [3] Andrea L Bertozzi and Mark Bowen. Thin film dynamics: theory and applications. In *Modern Methods in Scientific Computing and Applications*, pages 31–79. Springer, 2002.
 - [4] Sebastiano Boscarino, Francis Filbet, and Giovanni Russo. High order semi-implicit schemes for time dependent partial differential equations. *Journal of Scientific Computing*, 68(3):975–1001, 2016.
 - [5] S. Burnett, J. Kreger, H. Kristensen, and A. Stocker. Dynamics of particle-laden thin films: Viscous fluid on an incline. *CAM report 15-70*, 2015.
 - [6] R. Chhabra and J. Richardson. *Non-Newtonian flow in the process industries: fundamentals and engineering applications*. Butterworth-Heinemann, 1999.
 - [7] B. Cook. Theory for particle settling and shear-induced migration in thin-film liquid flow. *Phys. Rev. E*, 78:045303, 2008.
 - [8] B. Cook, A. Bertozzi, and A. Hosoi. Shock solutions for particle-laden thin films. *SIAM J. Appl. Math.*, 68:760–783, 2008.
 - [9] B. P. Cook, O. Alexandrov, and A. L. Bertozzi. Linear stability of particle-laden thin films. *Eur. Phys. J. Special Topics*, 166:77–81, 2009.
 - [10] Benjamin P Cook, Andrea L Bertozzi, and AE Hosoi. Shock solutions for particle-laden thin films. *SIAM Journal on Applied Mathematics*, 68(3):760–783, 2008.
 - [11] RV Craster and OK Matar. Dynamics and stability of thin liquid films. *Reviews of modern physics*, 81(3):1131, 2009.
 - [12] Harald Garcke and Sandra Wieland. Surfactant spreading on thin viscous films: nonnegative solutions of a coupled degenerate system. *SIAM journal on mathematical analysis*, 37(6):2025–2048, 2006.
 - [13] H. E. Huppert. Flow and instability of a viscous current down a slope. *Nature*, 300:427–429, 1982.
 - [14] O. Katz and E. Aharonov. Landslides in vibrating sand box: what controls types of slope failure and frequency magnitude relations? *Earth Planet. Sci. Lett.*, 247:280–294, 2006.
 - [15] L. Kondic. Instabilities in gravity driven flow of thin fluid films. *SIAM Review*, 45:95–115, 2003.
 - [16] Matthew R. Mata and Andrea L. Bertozzi. A numerical scheme for particle-laden thin film flow in two dimensions. *J. Comp. Phys.*, 230(16):6334–6353, 2011.
 - [17] A. Mavromoustaki and A. L. Bertozzi. Hyperbolic systems of conservation laws in gravity-driven, particle-laden thin-film flows. *J. Engineering Math.*, 88:29–48, 2014.
 - [18] Ryan M Miller and Jeffrey F Morris. Normal stress-driven migration and axial development in pressure-driven flow of concentrated suspensions. *Journal of non-newtonian fluid mechanics*, 135(2):149–165, 2006.
 - [19] C. Monquet, V. Greffeuille, and S. Treche. Characterization of the consistency of gruel’s consumed by infants in developing countries: assessment of the Bostwick consistometer and comparison with viscosity measurements and sensory perception. *Int J. Food Sci. Nutr.*, 57:459–469, 2006.
 - [20] N. Murisic, J. Ho, V. Hu, P. Latterman, T. Koch, K. Lin, M. Mata, and A.L. Bertozzi. Particle-laden viscous thin-films on an incline: Experiments compared with a theory based on shear-induced migration and particle settling. *Physica D: Nonlinear Phenomena*, 204(20):1661–1673, 2011.
 - [21] N. Murisic, B. Pausader, D. Peschka, and A.L. Bertozzi. Dynamics of particle settling and resuspension in viscous liquids. *J. Fluid Mech.*, 717:203–231, 2013.
 - [22] Prabhu R Nott, Elisabeth Guazzelli, and Olivier Pouliquen. The suspension balance model revisited. *Physics of Fluids*, 23(4):043304, 2011.
 - [23] Arun Ramachandran and David T Leighton. The influence of secondary flows induced by normal stress differences on the shear-induced migration of particles in concentrated suspensions. *Journal of Fluid Mechanics*, 603:207–243, 2008.
 - [24] Arun Ramachandran and David T Leighton. The influence of secondary flows induced by normal stress differences on the shear-induced migration of particles in concentrated suspensions. *Journal of Fluid Mechanics*, 603:207–243, 2008.
 - [25] M. Smith and S. Davis. Instabilities of dynamic thermocapillary liquid layers. Part i. Convective instabilities. *J. Fluid Mech.*, 132:119–144, 1983.
 - [26] Clyde E Stauffer. The measurement of surface tension by the pendant drop technique. *The Journal of Physical Chemistry*, 69(6):1933–1938, 1965.
 - [27] L. Wang and A. L. Bertozzi. Shock solutions for high concentration particle-laden thin films. *SIAM J. Appl. Math.*, 74:322–344, 2014.
 - [28] L. Wang, A. Mavromoustaki, A. L. Bertozzi, G. Urdaneta, and K. Huang. Rarefaction-singular shock dynamics for conserved volume gravity driven particle-laden thin film. *Phys. Fluids*, 27:033301, 2015.

- [29] Thomas Ward, Chi Wey, Robert Glidden, A. E. Hosoi, and A. L. Bertozzi. Experimental study of gravitation effects in the flow of a particle-laden thin film on an inclined plane. *Physics of Fluids*, 21:083305, 2009.
- [30] K Zhang and A Acrivos. Viscous resuspension in fully developed laminar pipe flows. *International journal of multiphase flow*, 20(3):579–591, 1994.
- [31] Liya Zhornitskaya and Andrea L Bertozzi. Positivity-preserving numerical schemes for lubrication-type equations. *SIAM Journal on Numerical Analysis*, 37(2):523–555, 1999.
- [32] J. Zhou, B. Dupuy, A. L. Bertozzi, and A. E. Hosoi. Theory for shock dynamics in particle-laden thin films. *Physical Review Letters*, 94:117803, 2005.